Neutron Shielding Simulations and Muon-induced Neutrons

Laura Vanhoefer[1], *Iris Abt*[1], *Lucia Garbini*[1], *Raphael Kneißl*[1], *Heng-Ye Liao*[1], *Béla Majorovits*[1], *Matteo Palermo*[1], *Oliver Schulz*[1]

[1]Max-Planck-Institut für Physik, Föhringer Ring 6, 80805 München, Germany

DOI: http://dx.doi.org/10.3204/DESY-PROC-2016-05/41

Cosmic-ray neutrons and muons can produce background in low-rate experiments due to the production of long-lived radioisotopes during transport above ground. This kind of background can be reduced by shielding the detector components during transport.
Cosmic-ray neutron and muon (μ^+ and μ^-) shielding simulations with the GEANT4 based framework MaGe were done to estimate the shielding properties of water, plastic, soil, steel, concrete, copper, LNGS rock and lead. The shielding power of cosmic-ray neutrons and muon-induced neutrons as well as the total neutron fluxes at different shielding depths are presented. Also the neutron backscattering effect was investigated and was found to be significant.

1 Introduction

Cosmic-ray neutrons and muons which are produced in the Earth's atmosphere can produce background in low-rate experiments like $0\nu\beta\beta$ experiments. Any energy deposition near or above the Q-value of the $0\nu\beta\beta$ decay is background for such experiments. Radioisotopes which produce such energy depositions can be created by neutrons and muons via spallation, neutron capture, (n,p) reaction etc. Also inelastic scattering where the nucleus is put into an excited state can produce an energy deposition near or above the Q-value. Long-lived radioisotopes with half-lives of many years are still present during measurements in an underground laboratory. This kind of background can be reduced by restricting the overall exposure to cosmic-ray radiation and by shielding of the detector components during transport above ground.
To compare different possible shielding materials, cosmic-ray neutron and muon shielding simulations were done using the GEANT4 based framework MaGe [1] from the GERDA and Majorana collaboration to estimate the shielding properties of plastic, water, soil, concrete, LNGS rock [2], steel, copper and lead (see also [3]).
In the simulations, blocks from different shielding materials were exposed to neutrons, μ^+ and μ^-. The number of neutrons and muons which leave the block at the other side are counted. Since the particles scatter inside the material, particles can scatter back whichs leads to multiple counting of particles. The investigation of the backscattering effect of neutrons is described in section 2. In section 3, the results of the neutron simulations are discussed. The results of the muon simulations are presented in section 4. Using the cosmic-ray neutron and muon-induced neutron fluxes, the total neutron flux can be calculated for each material. These results are shown in section 5.

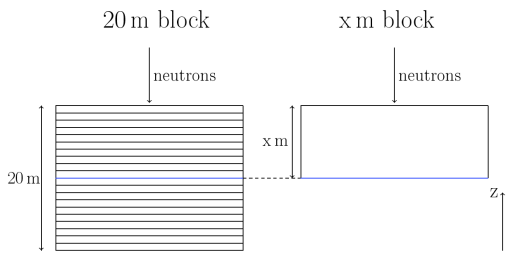

Figure 1: Illustration of the backscattering effect.

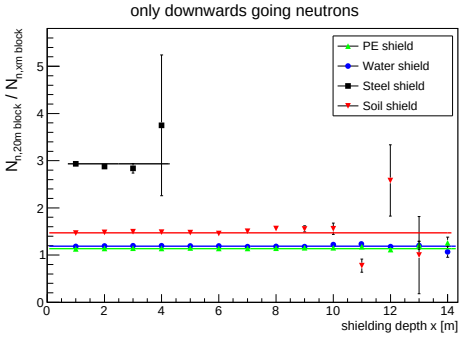

Figure 2: Ratio of neutrons counted inside a block and neutrons leaving blocks with different thicknesses.

Material	Plastic	Water	Soil	Steel
All neutrons	1.3552 ± 0.0006	1.4918 ± 0.0005	2.1718 ± 0.0005	5.340 ± 0.002
Downwards going neutrons	1.1370 ± 0.0005	1.1899 ± 0.0004	1.4723 ± 0.0004	2.9322 ± 0.0009
Upwards going neutrons	0.218 ± 0.001	0.3019 ± 0.0008	0.700 ± 0.001	2.408 ± 0.008

Table 1: Neutron flux inside a 20 m block at a certain shielding depth divided by the neutron flux behind a block with the corresponding thickness.

2 Backscattering effect

During particle transport in the simulation, the particle properties like momentum, energy and position are only stored if a boundary is crossed. Usually it is not monitored how often a particle crosses the same boundary. Therefore backscattering can lead to double or even multiple counting of neutrons. This can lead to wrong shielding indices. To estimate the fraction of backscattered neutrons, a 20 m block, which is divided into 20 sub-blocks, was simulated. The total neutron flux and the neutron flux pointing downwards are derived at different shielding depths inside the block. These numbers are then compared to the number of simulated neutrons leaving a block with the corresponding thickness. This is illustrated by Fig. 1. The ratio between the number of neutrons between the 20 m block and the block with the corresponding thickness is a measure of backscattering and is shown in Fig. 2. Without backscattering, the ratio would be one. The larger the ratio, the more neutrons scatter back. From Fig. 2 it can be seen that backscattering does not depend on the depth. Therefore the ratio can be obtained by averaging over all depths. The results are shown in Table 1. It can clearly be seen that backscattering is larger for denser materials with higher average mass number A like steel and that the backscattering effect is significant. Therefore one block for each shielding thickness has to be simulated. Further, the material blocks need to be placed in vacuum to avoid miscounting at the boundary of the block.

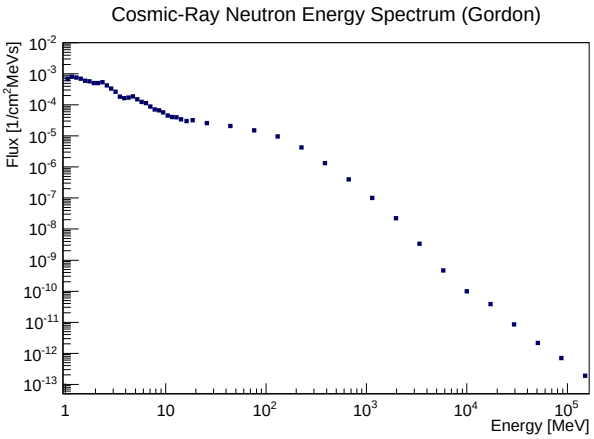

Figure 3: Used neutron energy spectrum. Datapoints are taken from [4].

3 Neutron simulations

For each shielding depth and material one block was simulated. Neutrons are injected following the energy spectrum shown in Fig. 3 measured by Gordon et al. [4]. Since the angular distribution of cosmic-ray neutrons is not well known, also the effect of using different angular distributions was investigated. For this purpose, a distribution where all neutrons are going only vertically downwards and an isotropic distribution were chosen, since the on average penetrated distance is the smallest for the first distribution and the largest for the second distribution. Also a distribution suggested by A. Nesterenok [5] for high-energetic cosmic-ray neutrons ($E \geq 10\,\mathrm{MeV}$) reaching the ground

$$J(\theta) = J_0 \exp[\alpha(1 - \cos\theta)] \qquad \text{with } \alpha = -2.5 \tag{1}$$

was investigated. In Eq. 1, J_0 is the flux in the vertical direction and θ is the nadir angle.
Figure 4 shows the energy spectra of cosmic-ray neutrons after penetrating steel blocks with different thicknesses. Only vertically downwards going neutrons were injected. A shielding thickness of 0 dm corresponds to the injected spectrum which is the Gordon spectrum shown in Fig 3. During penetration, neutrons lose energy by scattering off shielding material nuclei. Some neutrons are stopped, but also new neutrons and other particles are created. After a certain depth, the shower reaches equilibrium. When equilibrium is reached, the shape of the energy spectrum is not changing anymore and more particles are shielded than produced. In Fig. 4, it can be seen that the equilibrium for steel is reached after 6 dm of shielding. The depths at which equilibrium is reached is also listed in Table 2 for all simulated materials.
After the equilibrium is reached, the decreasing neutron flux with increasing shielding depth can be described by a power law fit [6]:

$$y = 10^{sx+a} \tag{2}$$

with the shielding depth x, the neutron flux $y(x)$, the shielding index s and a fit constant a.
Figure 5 shows the number of neutrons normalized to the number of arriving neutrons for different shielding depths and materials. The results of the power law fits are shown in Table 2.

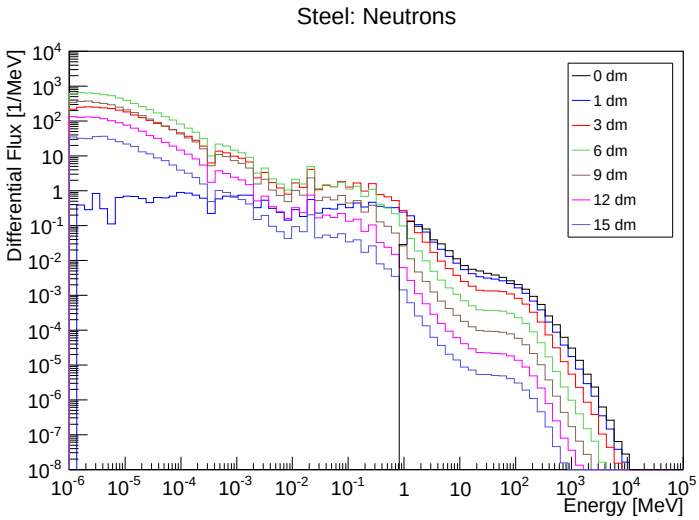

Figure 4: Simulated neutron energy spectrum at different depths for steel. Only downwards going neutrons were injected.

Material	EQ depth	Only downwards going neutrons	Nesterenok	Isotropic
Plastic	< 0.1	-0.354 ± 0.003	-0.366 ± 0.002	-0.388 ± 0.005
Water	< 0.1	-0.372 ± 0.003	-0.397 ± 0.007	-0.418 ± 0.005
Soil	< 0.1	-0.57 ± 0.01	-0.584 ± 0.007	-0.611 ± 0.009
Concrete	0.1 ± 0.05	-0.822 ± 0.006	-0.855 ± 0.004	-0.91 ± 0.02
LNGS rock	0.6 ± 0.05	-0.850 ± 0.003	-0.897 ± 0.005	-0.961 ± 0.009
Steel	0.6 ± 0.05	-2.01 ± 0.02	-2.12 ± 0.02	-2.22 ± 0.03
Copper	0.7 ± 0.05	-2.10 ± 0.02	-2.15 ± 0.01	-2.22 ± 0.02
Lead	1.6 ± 0.05	-1.368 ± 0.009	-1.39 ± 0.01	-1.42 ± 0.01

Table 2: Shielding index s [1/m] for different materials and angular distributions ($E \geq 0\,\text{MeV}$). The depth at which equilibrium of the shower is reached (EQ depth [m]) is also shown.

More neutrons are shielded if the shielding index is smaller. This is the case for denser materials with higher mass number A. Comparing the shielding indices of different angular distributions for the same material, it can be seen that the shielding indices of the isotropic distribution are always the smallest and the shielding indices of the only vertically downwards going neutron distribution is always larger. This can be explained by the fact that the on average penetrated distance is larger for the isotropic distribution. It can also be seen that the difference of the indices is smaller compared to the difference between different materials. This means that the influence of the chosen material is much larger than the influence of the injection angular distribution.

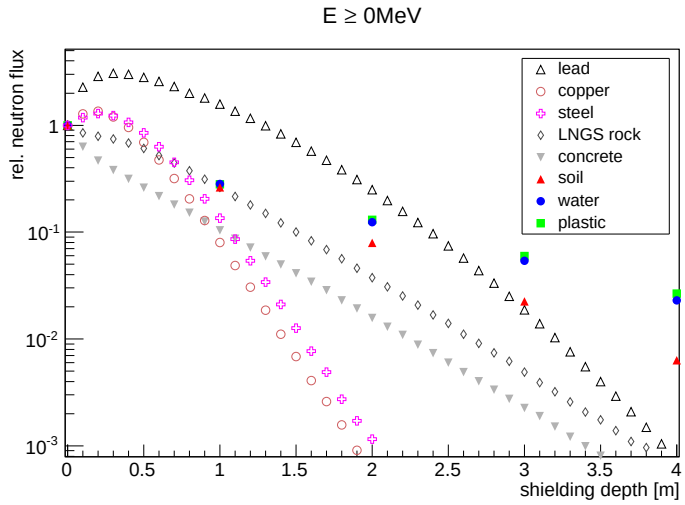

Figure 5: Simulated neutron flux at different shielding depths normalized to the incoming neutron flux for different materials. The angular distribution suggested by [5] (see Eq. 1) was used.

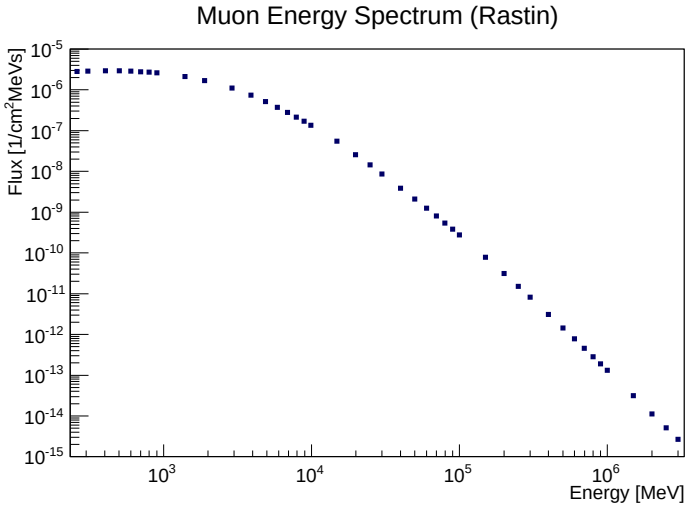

Figure 6: Used muon energy spectrum. Datapoints are taken from [7].

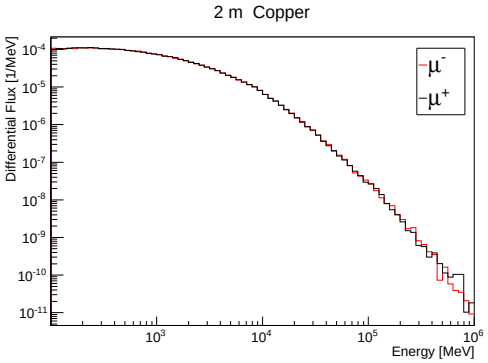

Figure 7: Comparison of the μ^- and μ^+ energy spectrum.

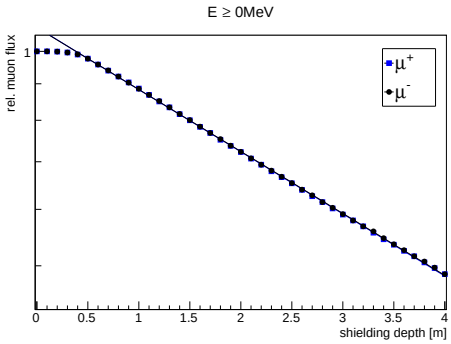

Figure 8: Muon flux at different shielding depths normalized to the incoming muons for LNGS rock.

4 Muon simulations

For the muon simulations the measured energy spectrum of Rastin [7], which is shown in Fig 6, was used as injection spectrum. Positive and negative charged muons were injected following a $\cos^2(\theta)$ angular distribution. Figure 7 compares the energy spectra of μ^+ and μ^- after the muons have penetrated 2 m of copper. It can clearly be seen that the energy spectra of μ^+ and μ^- are very similar. Also the number of muons at different shielding depths is the same which is shown by Fig. 8. This is expected since they undergo similar reactions. The only difference is that only μ^- can undergo muon capture. Low energetic μ^+ can only decay and can not be captured.
Muons induce neutrons during penetration. The number of neutrons normalized to the number of injected muons at different shielding depths is shown in Fig. 9. It can clearly be seen that the number of muon induced neutrons differs for μ^+ and μ^-. More neutrons are induced by μ^-. From looking at Fig. 8 it is evident that this can not be explained by different muon shielding properties, since the are the same for μ^+ and μ^-. The different amount of muon-induced neutrons can be explained by the fact that neutrons are produced during muon capture which only μ^- can undergo. During muon decay, no neutrons are produced.
From Fig. 9 it can also be seen that the difference between μ^+ and μ^--induced neutrons becomes smaller at larger shielding depths, where the number of stopping muons is also smaller (see [8]). Figure 10 compares the energy spectra of μ^+ and μ^--induced neutrons. The spectra differ since they are normalized with the number of induced neutrons which is smaller for μ^+. The shape of both energy spectra is similar up to a few MeV. Above few tens of MeV the differential fluxes are the same for μ^+ and μ^-.
The power law fit of Eq. 2 was applied for depths at which the shower is in equilibrium. The results are shown in Table 3. As expected the shielding indices for neutrons are smaller than the shielding indices for muon-induced neutrons. Therefore the muon-induced neutron flux starts to dominate the total neutron flux at larger shielding depths. Denser material with higher mass number A shields cosmic-ray neutrons more efficiently, but also more neutrons are produced. Therefore the total neutron flux has to be considered.

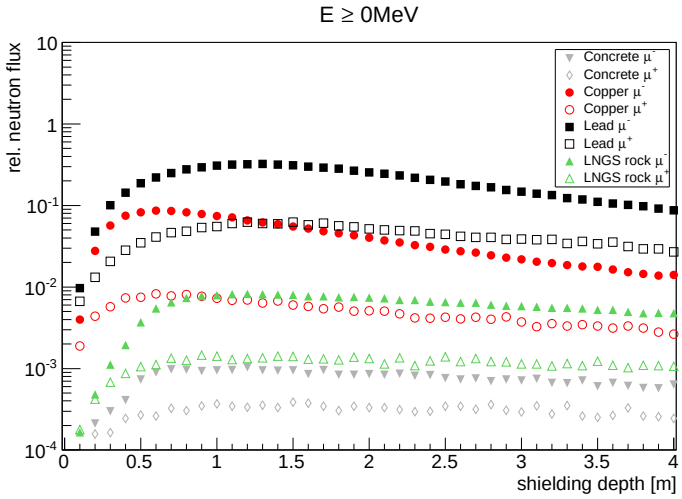

Figure 9: Muon-induced neutrons normalized to the incoming muons at different shielding depths for different materials.

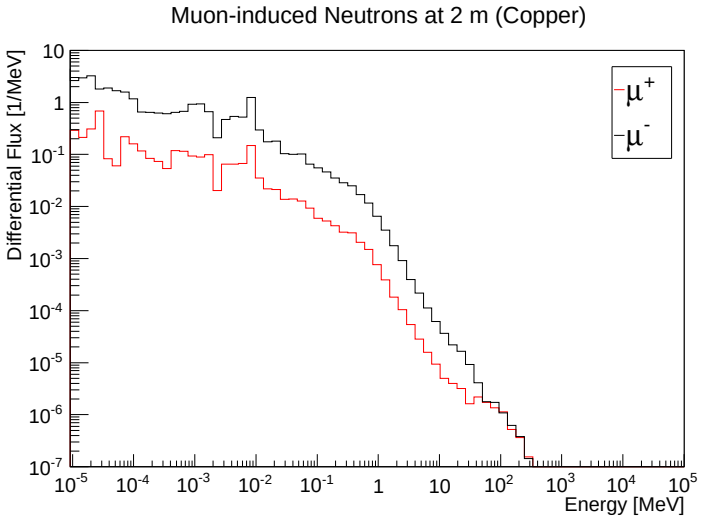

Figure 10: Comparison of the μ^--induced and μ^+-induced neutron energy spectrum.

Material	μ^+ [m^{-1}]	μ^- [m^{-1}]
Plastic	-0.0193 ± 0.0008	-0.0246 ± 0.0008
Water	-0.021 ± 0.001	-0.0271 ± 0.0007
Soil	-0.0264 ± 0.0009	-0.045 ± 0.001
Concrete	-0.041 ± 0.008	-0.079 ± 0.004
LNGS rock	-0.038 ± 0.006	-0.085 ± 0.003
Steel	-0.046 ± 0.004	-0.065 ± 0.002
Copper	-0.134 ± 0.005	-0.256 ± 0.003
Lead	-0.122 ± 0.006	-0.238 ± 0.002

Table 3: Shielding index s for muon-induced neutrons in [1/m] ($E \geq 0$ MeV).

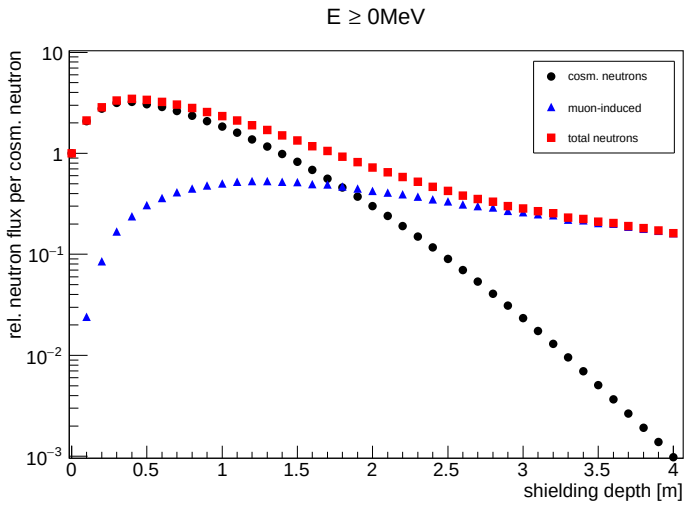

Figure 11: Neutron fluxes at different shielding depths for lead normalized to the incoming cosmic-ray neutrons. All cosmic-ray neutrons were injected vertically downwards going.

5 Total neutron flux

Using the results of the cosmic-ray neutron and muon simulations, the total neutron flux can be calculated. At sea-level, the ratio of neutrons to muons is 1:3 (see [9]). The muon charge ratio is $\mu^+/\mu^- \sim 1.25$ [10]. Therefore the neutron simulation results have to be weighted with a factor of 0.25, the μ^+ simulation results with a factor of 0.417 and the μ^- simulation results with a factor of 0.333 to get the total neutron flux.
Figure 11 shows the total neutron flux at different shielding depths of lead. Also the cosmic-ray and the total muon-induced neutron fluxes are shown. At smaller shielding depths, the total neutron flux is dominated by the cosmic-ray neutron flux. At larger depths, the flux is dominated by the muon-induced neutron flux.
In Fig. 12, the total neutron fluxes behind different materials is shown. Figure 13 shows the flux of neutrons with $E_n \geq 20$ MeV. It can be seen that the total flux is lowest behind a concrete shielding. This is not the case for neutrons with an energy higher than 20 MeV. There are less

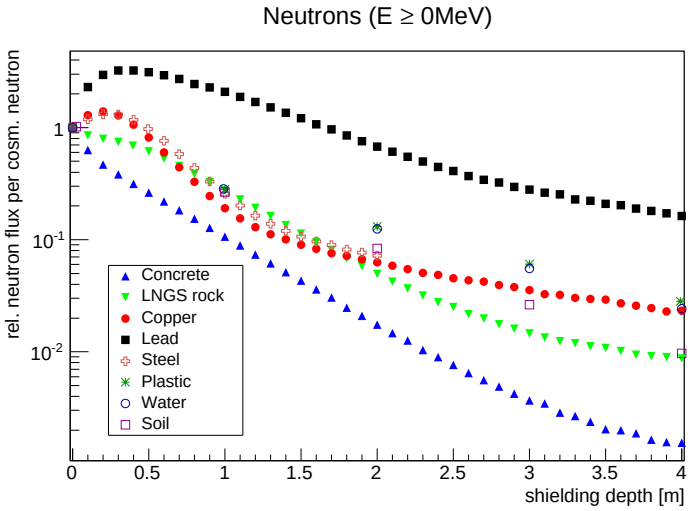

Figure 12: Total neutron flux at different shielding depths for different materials. The outgoing neutrons were normalized to the incoming cosmic-ray neutrons which were distributed by Eq. 1.

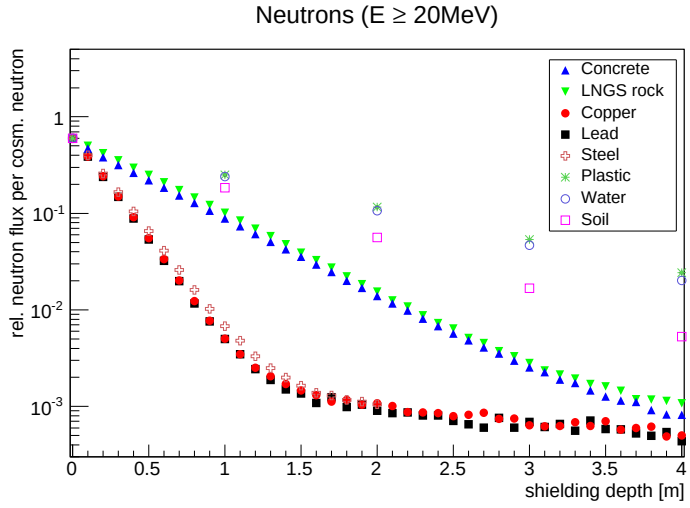

Figure 13: Total neutron flux at different shielding depths for different materials. The outgoing neutrons were normalized to the incoming cosmic-ray neutrons which were distributed by Eq. 1.

neutrons with $E_n \geq 20\,\mathrm{MeV}$ after copper, lead or steel shielding. This shows that the best choice of shielding material depends on the energy of neutrons which one likes to shield.

6 Conclusion

Cosmic-ray neutron and muons (μ^+ and μ^-) were simulated with the GEANT4 based framework MaGe to get the shielding powers of cosmic-ray neutrons and muon-induced neutrons for different shielding materials. More neutrons are induced by μ^- than by μ^+ due to muon capture. This difference becomes smaller at larger shielding depths, since also the number of stopping muons becomes smaller.
Denser material shields more cosmic-ray neutrons, but also more neutrons are induced. Therefore the total neutron flux has to be calculated to compare different materials. The best choice of shielding material depends on the energy of neutrons which one wants to be shielded.

References

[1] Melissa Boswell et al. MaGe-a Geant4-based Monte Carlo Application Framework for Low-background Germanium Experiments. *IEEE Trans. Nucl. Sci.*, 58:1212–1220, 2011.

[2] H. Wulandari, J. Jochum, W. Rau, and F. von Feilitzsch. Neutron flux underground revisited. *Astropart. Phys.*, 22:313–322, 2004.

[3] Laura Vanhoefer et al. Neutron Shielding Simulations and Muon-induced Neutrons. *PoS*, NEUTEL2015:085, 2015.

[4] Gordon M. S. et al. Measurement of the Flux and Energy Spectrum of Cosmic-Ray Induced Neutrons on the Ground. *IEEE Trans. Nucl. Sci.*, 51:3427–3434, 2004.

[5] Aleksandr Nesterenok. Numerical calculations of cosmic ray cascade in the Earth's atmosphere: Results for nucleon spectra. *Nucl. Instrum. Meth.*, B295:99–106, 2013.

[6] Aaron Michel. Investigation of cosmic ray shielding properties of different materials at shallow depths. diploma thesis, Technische Universität München, 2012.

[7] B. C. Rastin. AN ACCURATE MEASUREMENT OF THE SEA LEVEL MUON SPECTRUM WITHIN THE RANGE 4-GEV/C TO 3000-GEV/C. *J. Phys.*, G10:1609–1628, 1984.

[8] G. L. Cassiday, J. W. Keuffel, and J. A. Thompson. Calculation of the stopping-muon rate underground. *Phys. Rev.*, D7:2022–2031, 1973.

[9] G. Heusser. Low-radioactivity background techniques. *Ann. Rev. Nucl. Part. Sci.*, 45:543–590, 1995.

[10] W. R. Frazer, C. H. Poon, D. Silverman, and H. J. Yesian. Limiting fragmentation and the charge ratio of cosmic ray muons. *Phys. Rev.*, D5:1653–1657, 1972.